Optical self-cooling of a membrane oscillator in a cavity optomechanical experiment at room temperature

P. Vezio,[1] M. Bonaldi,[2,3] A. Borrielli,[2,3] F. Marino,[4,5] B. Morana,[2,6] P. M. Sarro,[6] E. Serra,[3,6] and F. Marin[1,7,5,4,*]

[1]*Dipartimento di Fisica e Astronomia, Università di Firenze, via Sansone 1, I-50019 Sesto Fiorentino (FI), Italy*
[2]*Nanoscience-Trento-FBK Division, Institute of Materials for Electronics and Magnetism, I-38123 Povo, Trento, Italy*
[3]*Trento Institute for Fundamental Physics and Application, Istituto Nazionale di Fisica Nucleare, I-38123 Povo, Trento, Italy*
[4]*CNR-INO, largo Enrico Fermi 6, I-50125 Firenze, Italy*
[5]*INFN, Sezione di Firenze, via Sansone 1, I-50019 Sesto Fiorentino (FI), Italy*
[6]*Department of Microelectronics and Computer Engineering/ECTM/DIMES, Delft University of Technology, Feldmanweg 17, NL-2628 CT Delft, The Netherlands*
[7]*European Laboratory for Non-Linear Spectroscopy, via Carrara 1, I-50019 Sesto Fiorentino (FI), Italy*

(Received 23 May 2023; accepted 28 November 2023; published 18 December 2023)

Thermal noise is a major obstacle to observing quantum behavior in macroscopic systems. To mitigate its effect, quantum optomechanical experiments are typically performed in a cryogenic environment. However, this condition represents a considerable complication in the transition from fundamental research to quantum technology applications. It is therefore interesting to explore the possibility of achieving the quantum regime in room-temperature experiments. In this work we test the limits of sideband-cooling vibration modes of a SiN membrane in a cavity optomechanical experiment. We obtain an effective temperature of a few millikelvins, corresponding to a phononic occupation number of around 100. We show that further cooling is prevented by the excess classical noise of our laser source, and we outline the road toward the achievement of ground state cooling.

DOI: 10.1103/PhysRevA.108.063508

I. INTRODUCTION

The research in the field of cavity optomechanics [1,2] has gained a lot of momentum in recent years, driven by the observation of quantum phenomena in optically cooled micro- and nanomechanical resonators. This breakthrough is paving the way for integrated systems implementing quantum measurements in sensing devices. In general, quantum properties of the optomechanical system are hidden or destroyed by thermal noise. As a consequence, most of the quantum optomechanical experiments performed to date have exploited resonators in a cryogenic environment [3–5]. However, this condition is a major obstacle to making usable sensors. Therefore, a recent branch of research is progressing toward a new generation of optomechanical systems, capable of maintaining quantum behavior and, in particular, approaching the mechanical ground state, even at room temperature. A disruptive impact has been achieved by systems based on levitated nanoparticles, whose oscillatory motion in optical tweezers has been cooled down to a phononic occupancy $\bar{n}$ below unity both with a passive scheme exploiting light scattered in a red-detuned cavity mode [6–8] and by measurement-based active feedback [9–11]. On the opposite side of the mass range, a phononic occupation number of $\bar{n} = 11$ was reported for the pendulumlike motion of the mirrors of the Laser Interferometer Gravitational-Wave Observatory (LIGO) [12]. Concerning deformation modes of micro- and nanodevices, active feedback cooling exploiting radiation pressure allowed us to cool a vibration mode of a nanometric string down to $\bar{n} = 27$ at room temperature [13] and $\bar{n} = 3.5$ in a liquid-nitrogen environment at 77 K [14]. The same technique led to similar results for a defect mode of a phononic crystal patterned on a SiN membrane, cooled down to $\bar{n} = 20$ [15] in a room-temperature experiment. A major achievement recently reported is the measurement and prediction of the motion of a defect mode of a membrane at room temperature with an accuracy corresponding to 0.97 quantum [16].

In this work we operate with a SiN membrane inside a high-finesse optical cavity [17] at room temperature, and unlike the cited works, we exploit passive, resolved-sideband cooling. This configuration has proven to be highly successful in the field of optomechanics. For instance, it is one of the first systems surpassing the threshold of $\bar{n} < 1$ in cryogenic experiments, both by means of sideband cooling [18,19] and with active feedback [20]. Having in mind easier application in future sensing devices, here we choose to realize a self-aligned, easily handled cavity. It requires no fine adjustment or gluing, and to elude electronic noise and improve mechanical accuracy we avoid piezoelectric transducers. These technical choices, together with the tuning range of our Nd:yttrium aluminum garnet (YAG) laser source, determine the requirements described in the next section. Our experiment and results are described in the following sections, where we show that we could achieve an effective temperature of a few millikelvins ($\bar{n}$ around 100), a limit well explained by a model including

*marin@fi.infn.it

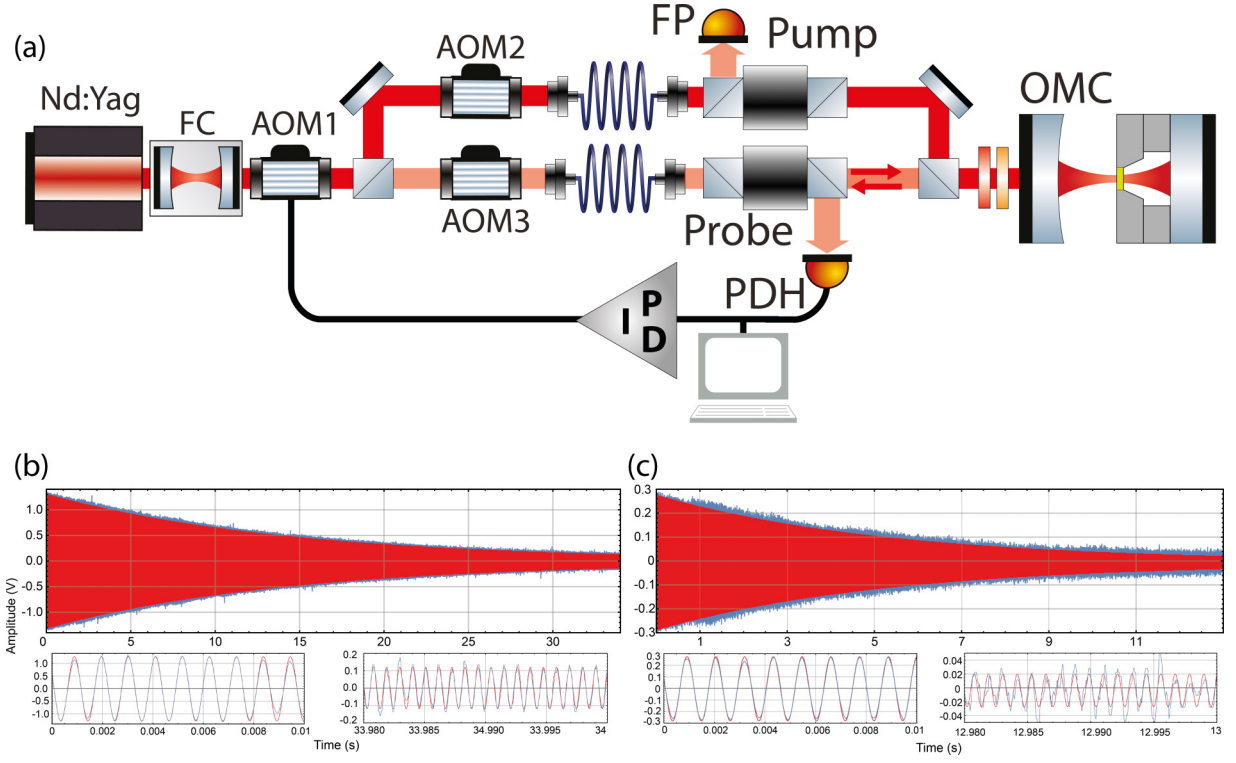

FIG. 1. (a) Simplified scheme of the experimental setup. FC: filter cavity; AOM: acousto-optic modulator; OMC: optomechanical cavity; PDH: Pound-Drever-Hall detection. (b) Ring-down signal of the (0,1) mode, frequency shifted by 257 kHz (blue) together with the fitting decaying sinusoidal function (red). On the bottom, enlarged views of the initial and final sectors are shown. (c) The same for the mode (0,2), shifted by 592 kHz.

excess laser noise, which is also crucial for providing reliable thermometry.

II. EXPERIMENTAL SETUP

A simplified scheme of the experimental setup is sketched in Fig. 1. The mechanical oscillator is a circular SiN membrane with a thickness of 100 nm and a diameter of 1.5 mm equipped with a specific on-chip structure that, working as a "loss shield" [21–24], reduces the coupling between the membrane and the frame and the consequent dissipation losses. In addition, the membrane thickness is reduced at the edge in order to further decrease the edge losses [25]. In this work we exploit the first two rotationally symmetric drum modes at $\Omega_m/2\pi \simeq 256$ kHz [mode (0,1)] and $\Omega_m/2\pi \simeq 593$ kHz [mode (0,2)].

The mechanical quality factors Q were measured from the ring-down of driven oscillations. We verified that Q depends meaningfully on the membrane cleanliness; therefore, for better accuracy we measured it with the membrane already mounted in the optical cavity in its final configuration, which is described below. To avoid perturbing optomechanical effects, we used for sensing a tunable, single-mode extended-cavity semiconductor laser operating around 970 nm, where the cavity finesse is below 100. The laser is frequency modulated at 20 MHz and locked to a cavity resonance using the reflected light, demodulated to obtain the first derivative of the Lorentzian dip. We verified by changing the locking point that the dynamical back-action of this probe laser is negligible. The same derivative signal is further mixed with a local oscillator at a frequency few hundred hertz apart from that of the selected mechanical mode, then low-pass filtered with a bandwidth of few kilohertz. The oscillation of each mode is thus selected and down-converted. A Nd:YAG laser, operating at a wavelength at which the finesse of the cavity is high, is tuned close to a cavity resonance to excite the mechanical modes by means of the radiation pressure. The Nd:YAG laser is then blocked, and the decaying signal is recorded. Two examples of such signals for the (0,1) and the (0,2) modes are shown in Fig. 1 together with the fitting damped oscillations. The measured quality factors are, respectively, $(1.18 \pm 0.03) \times 10^7$ and $(0.92 \pm 0.06) \times 10^7$, where the errors reflect one standard deviation over repeated measurements.

The configuration of the optomechanical cavity is dictated by two requirements: (a) it should be self-aligned, without position and tilt adjustments for the membrane and the mirrors, and (b) we want to avoid piezoelectric transducers. Due to the latter requirement, by tuning the laser source we have to optimize the position of the membrane with respect to the cavity standing wave and to find a resonance of the overall cavity. For what concerns the optical alignment, we have to consider that the membrane plane must be orthogonal to the cavity optical axis. To ensure it, we have implemented a cavity with a flat end mirror. Silicon spacers between the mirror and the membrane frame, obtained from high-quality wafers, guarantee the required parallelism between the surfaces of the mirror and the membrane [26,27]. In order to achieve good optomechanical coupling, we have to vary the

position of the membrane with respect to the cavity standing wave; therefore, the distance L_1 between the flat mirror and the membrane should be ideally at least $c/4\Delta\nu$ (c is the speed of light, and $\Delta\nu$ is the overall laser tuning range). In our case, $\Delta\nu \simeq 30\,\mathrm{GHz}$, and we have used two 1-mm-thick spacers, giving $L_1 = 2\,\mathrm{mm}$. To ensure that a cavity resonance is close to the optimal frequency, we require that the cavity length L_c is much larger than L_1. Moreover, to avoid scattering of the light impinging outside the membrane edge, it is important that the cavity waist is not too large. For this purpose, we have chosen a nearly hemispherical configuration, with a concave input coupler with a radius of 50 mm and a total cavity length of $L_c = 48\,\mathrm{mm}$ guaranteed by an Invar cylindrical spacer. The calculated beam waist is 50 μm on the flat mirror and 52 μm on the membrane, i.e., much smaller than the membrane diameter. The cavity finesse (defined as the ratio between the empty-cavity free spectral range and the optical linewidth), measured with the membrane under working conditions, is around 15 400, with an input coupler transmission of 330 ppm.

The cavity is positioned on a cantilever suspension system inside a vacuum chamber, evacuated down to 10^{-6} mbar. The emission of the Nd:YAG laser is frequency locked to a 22-cm-long filter cavity with a linewidth of 66 kHz. The slow branch of the feedback loop is sent to a piezoelectric transducer (PZT) moving one mirror of the filter cavity, while the fast branch controls the laser frequency by means of its internal PZT. The light transmitted by the filter cavity is tuned by a double-pass acousto-optic modulator (AOM) and split into two beams (the cooling and probe beams) whose frequency difference is set by two additional AOMs. The two beams are sent to the experimental bench by optical fibers, overlapped by orthogonal polarizations, and mode-matched to the optomechanical cavity. The reflected probe beam is used for frequency locking the laser to a cavity resonance by means of a Pound-Drever-Hall (PDH) detection and a servo loop acting on the first AOM, with a locking bandwidth of ∼10 kHz. To derive the PDH error signal, the probe beam is phase modulated at 13.3 MHz before it is coupled to the fiber.

The same PDH signal is also used to obtain the spectrum of the membrane motion. The power of the probe beam is around 100 μW. The PDH signal is converted into frequency fluctuations thanks to a calibration tone produced by adding a sinusoidal voltage with a frequency of 20 kHz to the correction signal going to the voltage-controlled oscillator that drives the first AOM. The cooling beam power is varied between 0 and ∼1 mW.

The frequency spectrum, corrected for the cavity filtering, can be used to deduce the single-photon optomechanical coupling rate g_0. As described in the next section, in the regime of moderate optomechanical cooling, when the thermal noise is the dominant source of force fluctuations, the peak area of the mechanical resonance can be written as $(g_0/2\pi)^2\,(2\,n_{\mathrm{eff}} + 1)$, where the phonon occupancy is $n_{\mathrm{eff}} = \frac{k_B T}{\hbar\Omega_m}\frac{\Gamma_m}{\Gamma_{\mathrm{eff}}}$ (k_B is the Boltzmann constant, T is the room temperature, $\Gamma_m = \Omega_m/Q$ is the natural mechanical width, Γ_{eff} is the measured peak width). Typical values of $g_0/2\pi$ are around 2 Hz for both modes.

III. MODEL

The role of excess phase and amplitude noise of the laser fields used for cooling and probing the mechanical oscillators was soon recognized by the optomechanical community, and its contribution to the achievable thermal occupation number was calculated, e.g., in Refs. [28–30]. These classical fluctuations manifest in the output field for two reasons: because they act as inherent noise and because the field probes the motion of the mechanical oscillator, which is, in turn, driven by fluctuations in intracavity intensity. As a consequence, the output spectrum is modified with respect to the case of coherent fields. The shape of the spectra obtained by heterodyne and direct intensity detection is derived in the literature, along with their correct use for thermometry [29–31]. In this section we recall and elaborate the results of a model of the optomechanical system including classical noise, described in detail in the Appendix, in order to clearly and correctly interpret our experimental spectra.

We consider a mechanical oscillator interacting with the field of an optical cavity with a decay rate κ and populated by an input field detuned by Δ from the cavity resonance. The mechanical and optical susceptibilities are defined as

$$\chi_m(\omega) = \frac{1}{-i(\omega - \Omega_m) + \Gamma_m/2}, \tag{1}$$

$$\chi_c(\omega) = \frac{1}{-i(\omega + \Delta) + \kappa/2}. \tag{2}$$

The optomechanical interaction modifies the susceptibility and the occupation number of the oscillator. The former can be written as

$$\chi_{\mathrm{eff}}(\omega) = \frac{1}{-i(\omega - \Omega_{\mathrm{eff}}) + \Gamma_{\mathrm{eff}}/2}, \tag{3}$$

where Ω_{eff} is the shifted resonance frequency, $\Gamma_{\mathrm{eff}} = \Gamma_{\mathrm{opt}} + \Gamma_m$, and Γ_{opt} is the optical damping. The oscillator occupancy is now

$$n_{\mathrm{eff}} = \frac{\Gamma_m}{\Gamma_{\mathrm{eff}}} n_{\mathrm{th}} + \frac{\Gamma_{\mathrm{opt}}}{\Gamma_{\mathrm{eff}}}(n_{\mathrm{ba}} + n_{\mathrm{exc}}), \tag{4}$$

where n_{th} is the occupancy of the thermal bath, which in our case is at room temperature; n_{ba} is the contribution of the quantum back-action; and n_{exc} is the contribution of sources of excess phase noise ϕ and relative amplitude noise ϵ, proportional to their spectral densities $S_{\phi\phi}$ and $S_{\epsilon\epsilon}$. As derived in the Appendix, the excess occupancy can be written as

$$n_{\mathrm{exc}} = \Gamma_{\mathrm{opt}} \frac{\Omega_m^2}{4g_0^2}\left(\frac{1}{\cos^2\theta} S_{\phi\phi} + A^2 S_{\epsilon\epsilon}\right), \tag{5}$$

with the definitions

$$\theta = \arg[\chi_c(\Omega_m) - \chi_c^*(-\Omega_m)] \tag{6}$$

and

$$A = \frac{|\chi_c^*(0)\chi_c(\Omega_m) + \chi_c(0)\chi_c^*(-\Omega_m)|}{\Omega_m |\chi_c(0)|^2\,\mathrm{Re}[\chi_c(\Omega_m) - \chi_c^*(-\Omega_m)]}. \tag{7}$$

The functions $1/\cos\theta$ and A are plotted in Fig. 2 for our experimental parameters κ and Ω_m.

In n_{eff}, the contribution of the thermal noise [first term on the right-hand side in Eq. (4)] is proportional to the inverse

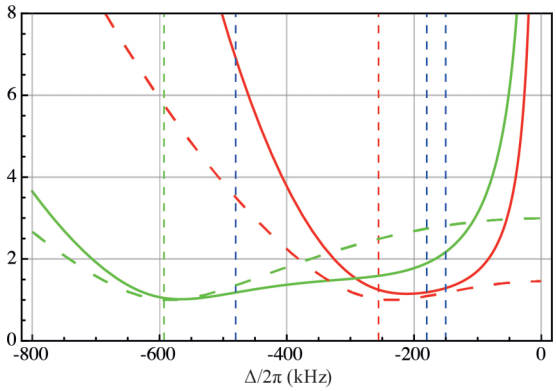

FIG. 2. Dimensionless functions $1/\cos\theta$ (dashed lines) and A (solid lines), described in the text, plotted as a function of the detuning $\Delta/2\pi$ for $\kappa/2\pi = 204$ kHz and $\Omega_m/2\pi = 256$ kHz (red curves) and 593 kHz (green curves). Vertical dotted lines correspond to $\Omega_m/2\pi$ (green and red lines) and the different values of detuning used in the present work (blue lines at −480, −180, and −150 kHz).

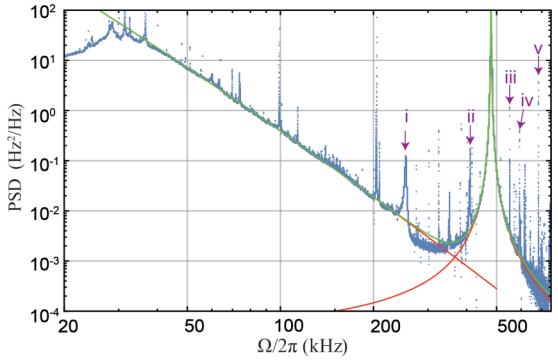

FIG. 3. Spectrum (power spectral density) of the PDH signal, calibrated in terms of frequency fluctuations. Red curves: fits of the low-frequency background and of the beat note between the probe and cooling beam. Green curve: overall background given by the sum of the two fitted curves. Purple arrows indicate the membrane modes, labeled (i) for mode (0,1), (ii) for (1,1), (iii) for (2,1), (iv) for (0,2), and (v) for (3,1).

of the input power (since $\Gamma_{\rm eff} \simeq \Gamma_{\rm opt}$, in turn, is proportional to the intracavity power), while the contribution of the excess noise [rightmost term in Eq. (4)] increases linearly with the input power. We can emphasize it by writing $n_{\rm eff}$ as

$$n_{\rm eff} = 0.5\, n_{\rm min}\left(\frac{\Gamma_{\rm opt}}{\Gamma_{\rm min}} + \frac{\Gamma_{\rm min}}{\Gamma_{\rm opt}}\right) + n_{\rm ba}, \tag{8}$$

where

$$n_{\rm min} = \frac{\Omega_m\sqrt{\Gamma_m n_{\rm th}}}{g_0}\sqrt{\frac{S_{\phi\phi}}{\cos^2\theta} + A^2 S_{\epsilon\epsilon}}. \tag{9}$$

We note that in the strongly resolved-sideband regime ($\kappa \ll \Omega_m$) and for $\Delta = -\Omega_m$, $\cos\theta$ and A assume their optimal values, $\cos\theta \simeq 1$ and $A \simeq 1$. In this case, the upper limits on the excess noise that allow us to achieve ground-state cooling (i.e., $n_{\rm min} < 1$) can be written in simple forms as $(2\pi)^2 S_{vv} < g_0^2/\Gamma_m n_{\rm th}$ [28] and $S_{\epsilon\epsilon} < g_0^2/\Omega_m^2\Gamma_m n_{\rm th}$, where the frequency-noise spectral density is $S_{vv} = (\omega/2\pi)^2 S_{\phi\phi}$.

For a given detuning, with varying input power the minimum occupancy is achieved when thermal noise and phase noise equally contribute $0.5 n_{\rm min}$, corresponding to the optimal optical width

$$\Gamma_{\rm min} = \frac{2g_0\sqrt{\Gamma_m n_{\rm th}}}{\Omega_m}\left(\frac{S_{\phi\phi}}{\cos^2\theta} + A^2 S_{\epsilon\epsilon}\right)^{-\frac{1}{2}}. \tag{10}$$

As derived in the Appendix, the output spectrum of a PDH detection can be written as

$$S_{\rm out} = c + |C(\omega)|^2\left[(2\pi)^2 S_{vv} + 2g_0^2\left(n_{\rm eff} + \frac{1}{2}\right)\mathcal{L} - 2g_0^2\, n_{\rm exc} 2\cos\theta(\cos\theta\,\mathcal{L} - \sin\theta\,\mathcal{D})\right], \tag{11}$$

where c is a constant accounting for the vacuum noise not entering the cavity (due, e.g., to the limited efficiency), the cavity filtering function is

$$C(\omega) = \frac{\kappa/2}{\kappa/2 - i\omega}, \tag{12}$$

and the Lorentzian and dispersive shapes $\mathcal{L}$ and $\mathcal{D}$ are, respectively,

$$\mathcal{L} = \frac{\Gamma_{\rm eff}}{2}[|\chi_{\rm eff}(\omega)|^2 + |\chi_{\rm eff}(-\omega)|^2] \tag{13}$$

and

$$\mathcal{D} = (\omega - \Omega_{\rm eff})|\chi_{\rm eff}(\omega)|^2 + (-\omega - \Omega_{\rm eff})|\chi_{\rm eff}(-\omega)|^2. \tag{14}$$

IV. EXPERIMENTAL RESULTS

Observing the detected spectrum over a wide frequency range (Fig. 3), we notice two relevant features: the tail of low-frequency fluctuations and the beat note between cooling and probe fields. The former is due to both frequency noise and low-frequency mechanical modes of the oscillator device belonging to the frame and to the internal filtering structure. We have observed that our filter cavity is efficient in reducing frequency noise above ∼100 kHz, but at a lower frequency, on the contrary, the noise increases [32]. The noise tail gives a contribution to the background beneath the peak of the first membrane mode at ∼260 kHz. The beat note is due to residual percolation between the two fields on the reflected path in spite of their orthogonal polarizations. This beat note is minimized using half- and quarter-wave plates before the cavity to compensate for its birefringence; however, the residual remains relevant. The two spectral structures are fitted with phenomenological shapes on frequency intervals outside the regions of the membrane modes, and the fitting functions are subtracted from the experimental spectra in order to minimize the residual background. We now focus on the first membrane mode, which appears in the spectra of the PDH detection. At low cooling power, the resonance peak is well fitted by a Lorentzian shape [Fig. 4(a)], which broadens at increasing cooling power. This broadening is accompanied at the beginning by a reduction in the peak area, but at high power the frequency noise plays a relevant role. The mode heats up again, and if $\cos\theta$ is not too small (depending on the detuning of the cooling field), the line shape is well reproduced by the sum of a Lorentzian curve and a dispersive

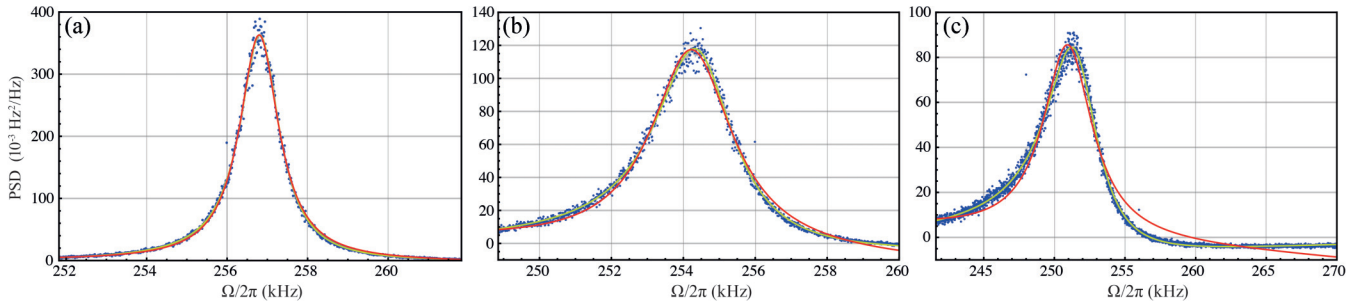

FIG. 4. Spectra of the resonance peak corresponding to the first membrane mode, acquired for a detuning of the cooling beam of $\Delta/2\pi = -480$ kHz, after the subtraction of the background shown in Fig. 3. (a)–(c) correspond to increasing cooling power, giving widths of $\Gamma_{\rm eff}/2\pi = 1.2$ kHz, $\Gamma_{\rm eff}/2\pi = 2.7$ kHz, and $\Gamma_{\rm eff}/2\pi = 9$ kHz, respectively. Dots: experimental data. Green solid line: fit with the sum of a Lorentzian and a dispersive shape [Eq. (15)]. Red solid line: fit with a Lorentzian shape [Eq. (15) with $a_3 = 0$].

curve, as predicted by Eq. (11). A clear example is shown in Fig. 4(c) for $\Delta = -480$ kHz. We remark that, after subtracting the background that includes c and the term directly proportional to S_{vv}, the remainder of the spectrum can be negative in a limited frequency region due to the contribution proportional to $\mathcal{D}$. The physical origin of this effect is the correlation between the frequency noise, which gives rise to intracavity radiation pressure noise, and the resulting oscillator motion, both imprinted in the fluctuations of the output field.

The calibrated output spectra, such as those shown in Fig. 4, are fitted with the function

$$a_0 + a_1\,\omega + |C(\omega)|^2(a_2\mathcal{L} + a_3\mathcal{D}), \tag{15}$$

where $\mathcal{L}$ and $\mathcal{D}$ are defined in Eqs. (13) and (14); a_i are free constant parameters; and $C(\omega)$, defined in Eq. (12), is completely determined by the independently measured κ. The terms $(a_0 + a_1\,\omega)$ account for the residual background remaining after the described subtraction of the low-frequency and beat-note structures. Comparing Eq. (15) with the theoretical spectrum given in Eq. (11), we deduce $a_2 = 2g_0^2(n_{\rm eff} + 1/2 - 2n_{\rm exc}\cos^2\theta)$ and $a_3 = 4g_0^2 n_{\rm exc}\cos\theta\sin\theta$. It is useful to define a new parameter $a_{\rm eff} = a_2 + a_3/\tan\theta$, which, following the comparison with Eq. (11), is equal to $a_{\rm eff} = g_0^2(2\,n_{\rm eff} + 1)$. θ is given by Eqs. (2) and (6), and it is calculated from independently measured system parameters. Finally, we fit $a_{\rm eff}$ vs $\Gamma_{\rm eff}$ with the function $a_{\rm eff} = b_1/\Gamma_{\rm eff} + b_2\Gamma_{\rm eff}$, with b_1 and b_2 being free parameters, a behavior that, according to Eq. (8), should hold for $\Gamma_{\rm opt} \simeq \Gamma_{\rm eff}$ and $n_{\rm min} \gg 1, n_{\rm ba}$. At low cooling power, the thermal noise dominates, and according to Eq. (4), we have $b_1 = 2g_0^2\,\Gamma_{\rm m} n_{\rm th}$. Since $\Gamma_{\rm m}$ and $n_{\rm th}$ are determined independently (the latter assuming that the oscillator is at room temperature), we can evaluate the optomechanical coupling rate g_0. The optimal width is derived as $\Gamma_{\rm min} = \sqrt{b_1/b_2}$, and the minimum occupation number is derived as $n_{\rm min} = 2\Gamma_{\rm m} n_{\rm th}\sqrt{b_2/b_1}$. In Fig. 5 we plot $a_{\rm eff}/2g_0^2 \equiv n_{\rm eff}$ for a detuning of the cooling beam of -480 kHz. With the described procedure, we derive $g_0/2\pi = 2.1 \pm 0.1$ Hz and $n_{\rm min} = 450 \pm 35$ at the optimal effective width of $\Gamma_{\rm min}/2\pi = 2.35$ kHz. The acquired spectrum corresponding to the lowest occupancy is shown in Fig. 4(b).

The excess occupation number $n_{\rm exc}$ is produced by both phase and amplitude excess noise. The coefficient of the dispersive shape, which is just sensitive to phase noise, allows distinguishing the two sources. According to Eq. (11), the contribution of the phase noise to $b_2\Gamma_{\rm eff}$ should be equal to $a_3/\sin 2\theta$, while a larger b_2 can be attributed to the amplitude noise. In our case, we find $b_2\Gamma_{\rm eff}/a_3 = -2.3 \pm 0.4$, in good agreement with the calculated $1/\sin 2\theta = -1.84$. As a consequence, we can ascribe $n_{\rm exc}$ to the excess phase noise. Using Eq. (9), we deduce a frequency noise of $S_{vv} = (2.2 \pm 0.4) \times 10^{-2}\,{\rm Hz}^2/{\rm Hz}$ around a mode eigenfrequency of $\sim$250 kHz. For the relative amplitude noise, we infer an upper limit of $S_{\epsilon\epsilon} < 2 \times 10^{-14}\,{\rm Hz}^{-1}$.

Following the behavior of $1/\cos\theta$ shown in Fig. 2, we infer that the minimum occupation number is potentially reduced by a factor of 4.4, i.e., down to $\sim$100, when the detuning is close to $\Delta \simeq -\Omega_{\rm m} \simeq -2\pi \times 260$ kHz. This working point implies two technical issues in the measurement of the phonon number. First, the beat note between the cooling and probe fields is close to the mechanical peak, hindering its accurate analysis. Second, here $|\sin\theta|$ is small; therefore, it is difficult to determine the weight of the dispersive contribution in the spectral shape and, consequently, the correction to be applied to the Lorentzian amplitude. We have, however, acquired sets of spectra at varying cooling powers for detunings of $\Delta/2\pi = -150$ kHz and $\Delta/2\pi = -180$ kHz. The deduced optomechanical coupling rate is now $g_0/2\pi = 2.6$ Hz, and the slight increase with respect to the previous value can be attributed to a different position of the membrane with respect to the cavity standing wave, caused by thermal drifts (these datasets were acquired on a different day than the previous ones). The inferred frequency noise is $S_{vv} = (2.2 \pm 1.3) \times 10^{-2}\,{\rm Hz}^2/{\rm Hz}$ for the data at $\Delta/2\pi = -150$ kHz and $S_{vv} = (3.0 \pm 1.4) \times 10^{-2}\,{\rm Hz}^2/{\rm Hz}$ for the data at $\Delta/2\pi = -180$ kHz, while the minimum occupation number is, respectively, $n_{\rm min} = 120 \pm 70$ and $n_{\rm min} = 130 \pm 60$. Even with the anticipated low accuracy, these results agree with the previously reported data, confirming the overall self-consistency of our modeling. We now consider the (0,2) mode of the membrane. Thanks to its higher resonance frequency (about 593 kHz), it has a lower back-action-limited occupation number $n_{\rm ba}$, and it is less sensitive to low-frequency technical noise. However, cavity filtering reduces the signal-to-noise ratio in the PDH detection. An example of the resonance peak acquired at moderate cooling is shown in Fig. 6(a) for a detuning of $\Delta/2\pi = -480$ kHz. The dispersive contribution to the line shape cannot be singled out. Even at the highest cooling power that still allows the resonance peak to be

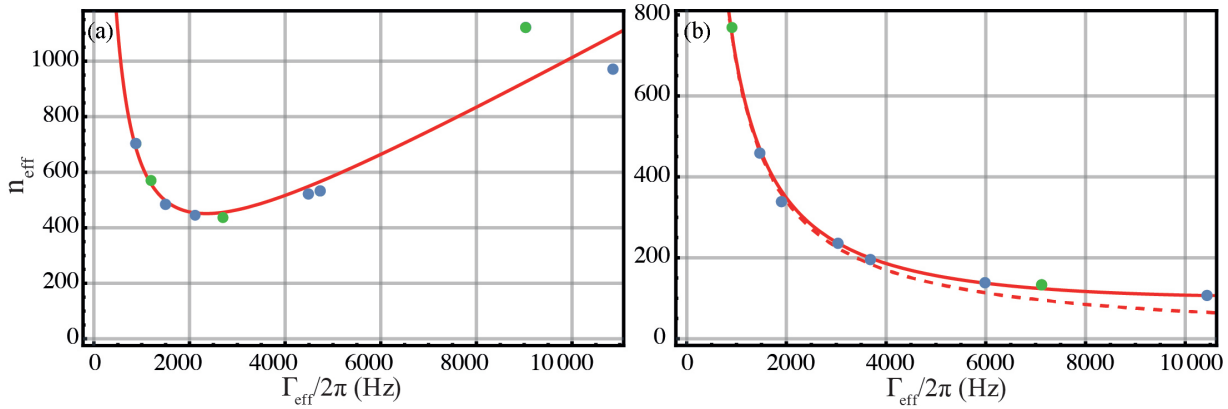

FIG. 5. Dots: area of the resonance peak of (a) the (0,1) mode and (b) the (0,2) mode of the membrane, calibrated in terms of thermal occupancy, at increasing cooling power, plotted as a function of the peak width. Green dots correspond to the spectra shown in Figs. 4 and 6. The red solid line show the fit with the function $b_1/\Gamma_{\rm eff} + b_2\Gamma_{\rm eff}$. The dashed line shows the $b_1/\Gamma_{\rm eff}$ contribution to the fit.

reliably extracted from the wings of the beat note, the purely Lorentzian shape gives the best fit to the experimental data, as shown in Fig. 6(b) and confirmed by the lack of visible systematic behavior in the fit residuals. The peak area, calibrated as before in terms of occupation number, is plotted in Fig. 5(b) as a function of the peak width $\Gamma_{\rm eff}$ and fitted with the function $b_1/\Gamma_{\rm eff} + b_2\Gamma_{\rm eff}$. We infer $g_0/2\pi = 1.74 \pm 0.02$ Hz and $n_{\rm min} = 104 \pm 14$ at the optimal effective width of $\Gamma_{\rm min}/2\pi = 13 \pm 2$ kHz.

The lack of a dispersive component in the peak line shape indicates that the frequency noise plays a negligible role, and $n_{\rm exc}$ should be imputed to the excess amplitude noise. Using Eq. (9) we infer $S_{\epsilon\epsilon} = (1.6 \pm 0.2) \times 10^{-14}\,{\rm Hz}^{-1}$. According to the behavior of A, an optimized detuning ($\Delta \simeq -\Omega_{\rm m}$) would reduce $n_{\rm eff}$ by 20%.

V. CONCLUSIONS

We have optically cooled two low-frequency vibration modes of a membrane at room temperature, exploiting self-cooling in a cavity optomechanical setup with a red-detuned cooling beam in the resolved-sideband regime. We have chosen to build a monolithic cavity, self-aligned, without including mechanical adjustments or piezoelectric transducers. For both modes we have achieved a phononic occupation number around 100, corresponding to effective temperatures of 1.5 and 3 mK for the (0,1) and (0,2) modes, respectively, and effective quality factors between 30 and 50. We have shown that this performance is limited by the laser excess noise. Without changing other parameters, lower occupation numbers could be obtained with oscillators exhibiting a higher quality factor, but achieving an occupancy of around 1 would require $Q \sim 10^{11}$, well above the state of the art for room-temperature membrane oscillators.

The excess amplitude noise can be reduced using an additional noise eater. In [33] we reported an active stabilization that reduces the intensity fluctuations at a level that is 3 dB above shot noise for a laser power of 24 mW. This corresponds to $S_{\epsilon\epsilon} = 0.8 \times 10^{-17}\,{\rm Hz}^{-1}$, i.e., more than three orders of magnitude lower than in the present experiment. We notice, however, that the intensity noise directly measured on our cooling beam is already lower than the $S_{\epsilon\epsilon}$ deduced from

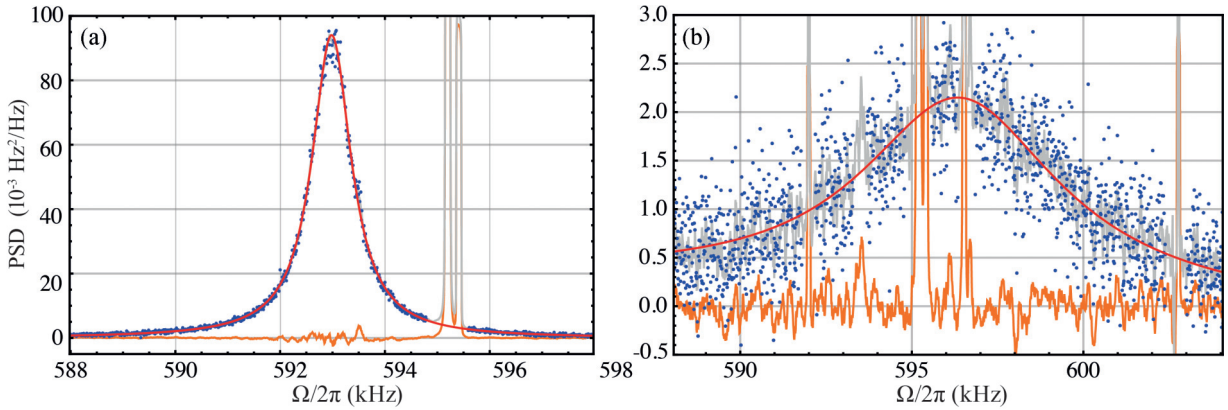

FIG. 6. Spectra of the resonance peak corresponding to the (0,2) membrane mode, acquired for a detuning of the cooling beam of $\Delta/2\pi = -480$ kHz. (a) and (b) correspond to increasing cooling power, giving widths of $\Gamma_{\rm eff}/2\pi = 900$ Hz and $\Gamma_{\rm eff}/2\pi = 7.1$ kHz, respectively. Blue dots: experimental data used for the fit. Light gray line: 10-point (equivalent to 100 Hz) moving average of the complete set of experimental data. A few spurious peaks are removed from the set used for the fit. Red solid line: fit with a Lorentzian shape. Orange solid line: residuals of the fit (10-point moving average).

the behavior of the (0,2) mode peak area. The intracavity excess intensity fluctuations may be caused by pointing noise, a technical issue that can be solved with a careful analysis of the optical path.

The excess frequency noise is a bigger problem. At present, we show that it limits the cooling performance for the (0,1) mode, but it is likely to similarly affect the (0,2) mode as soon the amplitude noise is reduced. For this second mode, a frequency noise below $0.7 \times 10^{-2}\,\mathrm{Hz}^2/\mathrm{Hz}$ is, indeed, required to drop n_{eff} below 100. A possible strategy to mitigate the effect of the excess frequency noise is to reduce the cavity length and, consequently, increase the optomechanical coupling rate. This comes at the price of dropping the design of a cavity without a piezoelectric transducer, at least when using a Nd:YAG laser source, due to a cavity free spectral range exceeding the laser tuning range. By decreasing the input mirror transmission down to 100 ppm one could shorten the cavity by a factor of 20, maintaining an overcoupled cavity with the mechanical modes in the resolved-sideband regime (thus ensuring $n_{\mathrm{ba}} < 1$). A phonon occupancy of around 7 then seems achievable with current oscillator parameters and laser excess noise, at least for the (0,2) mode. The effective quality factor would, however, drop to ∼3, an unreasonable value if we consider the presence of the other mechanical modes and the low-frequency background. A level of n_{eff} around or slightly below 20, dominated by the thermal noise, is more realistically within reach.

To arrive at the so-called ground-state level $n_{\mathrm{eff}} \simeq 1$, the quality factor of the membrane modes should then be increased above 10^8, a threshold already achieved in thinner membranes isolated from the frame by tethers [34] or patterned phononic crystals [15,35]. We remark that the fluctuations in the cavity length could now play a relevant role. Their effect is equivalent to that of laser frequency noise, with spectral density scaling as $S_{LL} = (L_c/\nu_{\mathrm{l}})^2 S_{\nu\nu}$ where ν_{l} is the laser frequency. In particular, to approach $n_{\mathrm{eff}} = 1$, we require S_{LL} below $10^{-36}\,\mathrm{m}^2/\mathrm{Hz}$. In [33] we reported an upper limit to the displacement noise of $\sim 10^{-36}\,\mathrm{m}^2/\mathrm{Hz}$ around 170 kHz for a 1.5-mm-long cavity, including a piezoelectric transducer, at cryogenic temperature. At room temperature, the mechanical modes of the bulky input mirror give a structured spectral background varying between 10^{-36} and $10^{-34}\,\mathrm{m}^2/\mathrm{Hz}$ in our frequency region of interest [36]. The calculated broadband Brownian noise of the mirror is around $10^{-37}\,\mathrm{m}^2/\mathrm{Hz}$ [37], and similar or lower levels are expected for thermoelastic and thermorefractive noise [38–40]. The low-frequency thermal noise of high-order membrane modes also plays a relevant role. Our finite-element-model simulations predict a background of $3 \times 10^{-36}\,\mathrm{m}^2/\mathrm{Hz}$ for the current device, but a lower level can be reached for membranes with a higher quality factor. Moreover, intermodulation radiation pressure noise produced by the nonlinearity of the cavity response function [41,42] must be attentively considered. The target is therefore not out of reach, but it requires careful evaluation of the displacement-noise background.

ACKNOWLEDGMENTS

Research was performed within the Project QuaSeRT funded by the QuantERA ERA-NET Cofund in Quantum Technologies implemented within the European Union's Horizon 2020 program. We also acknowledge financial support from PNRR MUR Project No. PE0000023-NQSTI.

APPENDIX

The linearized evolution equations for the intracavity field operator $\delta\hat{a}$ and the mechanical bosonic operator $\hat{b}$, in the frame rotating with angular frequency $\omega_{\mathrm{l}} = 2\pi\nu_{\mathrm{l}}$ (ν_{l} is the laser frequency), are [1]

$$\delta\dot{\hat{a}} = \left(i\Delta - \frac{\kappa}{2}\right)\delta\hat{a} + ig_0\,\alpha(\hat{b} + \hat{b}^\dagger) + \sqrt{\kappa}\,\delta\hat{a}_{\mathrm{in}}, \tag{A1}$$

$$\dot{\hat{b}} = \left(-i\Omega_{\mathrm{m}} - \frac{\Gamma_{\mathrm{m}}}{2}\right)\hat{b} + ig_0(\alpha^*\delta\hat{a} + \alpha\delta\hat{a}^\dagger) + \sqrt{\Gamma_{\mathrm{m}}}\,\hat{b}_{\mathrm{in}}, \tag{A2}$$

where $\Delta = \omega_{\mathrm{l}} - \omega_{\mathrm{c}}$ is the detuning with respect to the cavity resonance frequency ω_{c}, κ and Γ_{m} are the optical and mechanical decay rates, α is the intracavity mean field, and the input terms are defined below.

In Fourier space, Eqs. (A1) and (A2) can be written as

$$\frac{1}{\chi_{\mathrm{c}}}\tilde{a} = ig_0\,\alpha\left(\tilde{b} + \tilde{b}^\dagger\right) + \sqrt{\kappa}\,\tilde{a}_{\mathrm{in}}, \tag{A3}$$

$$\frac{1}{\chi_{\mathrm{m}}}\tilde{b} = ig_0\left(\alpha^*\tilde{a} + \alpha\tilde{a}^\dagger\right) + \sqrt{\Gamma_{\mathrm{m}}}\,\tilde{b}_{\mathrm{in}}, \tag{A4}$$

where we use $\tilde{O}$ to indicate the Fourier transform of the operator $\hat{O}$ and $\tilde{O}^\dagger$ for the Fourier transform of $\hat{O}^\dagger$, such that $[\tilde{O}(\omega)]^\dagger = \tilde{O}^\dagger(-\omega)$. The optical and mechanical susceptibilities are defined in Eqs. (1) and (2), and the intracavity mean field α is related to the input field α_0 by the equation $\alpha = \sqrt{\kappa}\chi_{\mathrm{c}}(0)\alpha_0$.

Replacing Eq. (A3) in Eq. (A4) and neglecting the counterrotating terms, the solution for $\tilde{b}$ can be written as

$$\frac{1}{\chi_{\mathrm{eff}}}\tilde{b} = ig_0\sqrt{\kappa}[\alpha^*\chi_{\mathrm{c}}(\omega)\tilde{a}_{\mathrm{in}} + \alpha\,\chi_{\mathrm{c}}^*(-\omega)\tilde{a}_{\mathrm{in}}^\dagger] + \sqrt{\Gamma_{\mathrm{m}}}\,\tilde{b}_{\mathrm{in}}, \tag{A5}$$

where the effective susceptibility χ_{eff} is defined as

$$\begin{aligned}\frac{1}{\chi_{\mathrm{eff}}} &= \frac{1}{\chi_{\mathrm{m}}} + g_0^2\,|\alpha|^2[\chi_{\mathrm{c}}(\omega) - \chi_{\mathrm{c}}^*(-\omega)] \\ &\simeq i(\Omega_{\mathrm{eff}} - \omega) + \frac{\Gamma_{\mathrm{eff}}}{2}.\end{aligned} \tag{A6}$$

The resonance frequency is shifted to

$$\Omega_{\mathrm{eff}} = \Omega_{\mathrm{m}} + g_0^2|\alpha|^2\,\mathrm{Im}[\chi_{\mathrm{c}}(\Omega_{\mathrm{m}}) - \chi_{\mathrm{c}}^*(-\Omega_{\mathrm{m}})] \tag{A7}$$

by the optical spring effect, and red-detuned radiation provides optical damping with the rate

$$\Gamma_{\mathrm{opt}} = 2g_0^2\,|\alpha|^2\,\mathrm{Re}[\chi_{\mathrm{c}}(\Omega_{\mathrm{m}}) - \chi_{\mathrm{c}}^*(-\Omega_{\mathrm{m}})], \tag{A8}$$

yielding a total width $\Gamma_{\mathrm{eff}} = \Gamma_{\mathrm{m}} + \Gamma_{\mathrm{opt}}$.

The input field fluctuations, including the classical extra phase and amplitude noise, can be written as

$$\delta\hat{a}_{\mathrm{in}} = \hat{a}_{\mathrm{v}} + \alpha_0\,(i\phi + \epsilon), \tag{A9}$$

where $\hat{a}_{\mathrm{v}}$ is a vacuum field operator and the phase and relative amplitude fluctuations are given by the classical, real stochastic variables ϕ and ϵ, which we assume are uncorrelated.

The input noise operators are characterized by the correlation functions

$$\langle \hat{a}_{\rm v}(t)\hat{a}_{\rm v}^{\dagger}(t')\rangle = \delta(t-t'), \tag{A10}$$

$$\langle \hat{a}_{\rm v}^{\dagger}(t)\hat{a}_{\rm v}(t')\rangle = 0, \tag{A11}$$

$$\langle \hat{b}_{\rm in}(t)\hat{b}_{\rm in}^{\dagger}(t')\rangle = (n_{\rm th}+1)\,\delta(t-t'), \tag{A12}$$

$$\langle \hat{b}_{\rm in}^{\dagger}(t)\hat{b}_{\rm in}(t')\rangle = n_{\rm th}\,\delta(t-t'), \tag{A13}$$

where $n_{\rm th}$ is the thermal occupation number of the thermal bath, which in our case is at room temperature.

Inserting the expressions of the input field noise in Eq. (A5), we derive

$$\begin{aligned}\frac{1}{\chi_{\rm eff}}\tilde{b} &= ig_0\sqrt{\kappa}[\alpha^*\chi_{\rm c}(\omega)\tilde{a}_{\rm v} + \alpha\chi_{\rm c}^*(-\omega)\tilde{a}_{\rm v}^{\dagger}] \\ &\quad - g_0\sqrt{\kappa}\alpha_0[\alpha^*\chi_{\rm c}(\omega) - \alpha\chi_{\rm c}^*(-\omega)]\tilde{\phi} \\ &\quad + ig_0\sqrt{\kappa}\alpha_0[\alpha^*\chi_{\rm c}(\omega) + \alpha\chi_{\rm c}^*(-\omega)]\tilde{\epsilon} + \sqrt{\Gamma_{\rm m}}\,\tilde{b}_{\rm in}.\end{aligned} \tag{A14}$$

The effective thermal occupation number can be calculated as $n_{\rm eff} = \int\!\!\int \langle \tilde{b}^{\dagger}(\omega')\tilde{b}(\omega)\rangle \frac{{\rm d}\omega'}{2\pi}\frac{{\rm d}\omega}{2\pi}$, leading to the weak-coupling limit

$$n_{\rm eff} = \frac{\Gamma_{\rm m}}{\Gamma_{\rm eff}}n_{\rm th} + \frac{\Gamma_{\rm opt}}{\Gamma_{\rm eff}}(n_{\rm ba}+n_{\rm exc}), \tag{A15}$$

where the contribution due to the quantum back-action is [1]

$$n_{\rm ba} = \left(\frac{(\kappa/2)^2+(\Delta-\Omega_{\rm m})^2}{(\kappa/2)^2+(\Delta+\Omega_{\rm m})^2} - 1\right)^{-1} \tag{A16}$$

and the contribution of the excess noise is

$$\begin{aligned}n_{\rm exc} = \frac{\kappa^2 g_0^2\alpha_0^4}{\Gamma_{\rm opt}}&[|\chi_{\rm c}^*(0)\chi_{\rm c}(\Omega_{\rm m}) - \chi_{\rm c}(0)\chi_{\rm c}^*(-\Omega_{\rm m})|^2\, S_{\phi\phi} \\ &+ |\chi_{\rm c}^*(0)\chi_{\rm c}(\Omega_{\rm m}) + \chi_{\rm c}(0)\chi_{\rm c}^*(-\Omega_{\rm m})|^2\, S_{\epsilon\epsilon}].\end{aligned} \tag{A17}$$

Using Eq. (A8) to replace α_0 in the above expression, the excess occupation number can be written in a simple form that is useful for the comparison with the experimental results as

$$n_{\rm exc} = \Gamma_{\rm opt}\frac{\Omega_{\rm m}^2}{4g_0^2}\left(\frac{1}{\cos^2\theta}\,S_{\phi\phi} + A^2 S_{\epsilon\epsilon}\right), \tag{A18}$$

where θ and A are defined in Eqs. (6) and (7).

The state of the oscillator is measured through the output field, which is given by the input-output relation $a_{\rm out} = -\sqrt{\kappa}a + a_{\rm in}$. For the field fluctuations, inserting Eq. (A3) in this latter relation, we can write

$$\tilde{a}_{\rm out} = -ig_0\,\alpha\,\chi_{\rm c}(\omega)\sqrt{\kappa}(\tilde{b}+\tilde{b}^{\dagger}) + [1-\kappa\chi_{\rm c}(\omega)]\tilde{a}_{\rm in}, \tag{A19}$$

and for the mean field $\alpha_{\rm out} = [1-\kappa\chi_{\rm c}(0)]\alpha_0$.

In order to gather information on the displacement of the oscillator, we analyze a quadrature of the probe field. In particular, in the case of PDH detection, the phase modulation sidebands act as a local oscillator to extract the phase quadrature of the resonant carrier field of the probe beam. We assume that all the fields (cooling field, probe, and local oscillator) are derived from the same laser source and are affected by the same excess phase and relative amplitude noise.

For a general quadrature detection, the total detected fluctuations are proportional to

$$X_{\rm out} = \tfrac{1}{2}\left(e^{-i(\theta_{\rm LO}+\phi)}\,a_{\rm out,p} + {\rm H.c.}\right) \simeq \tfrac{1}{2}\left(e^{-i\theta_{\rm LO}}\tilde{a}_{\rm tot} + {\rm H.c.}\right), \tag{A20}$$

where $\theta_{\rm LO}$ is the phase of the local oscillator, $\tilde{a}_{\rm tot} = \tilde{a}_{\rm out,p} - i\alpha_{\rm out,p}\phi$, and we use the subscript p for the probe field. Neglecting the quantum noise of the probe and using Eqs. (A9) and (A19), the total detected field, after some algebra and noting, in particular, that $\chi_{\rm c}^{-1}(0) - \chi_{\rm c}^{-1}(\omega) = i\omega$, can be written as

$$\begin{aligned}\tilde{a}_{\rm tot} &= -i\alpha_{0,\rm p}\kappa\,\chi_{\rm c,p}(\omega)\chi_{\rm c,p}(0)[i\omega\tilde{\phi} + g_0(\tilde{b}+\tilde{b}^{\dagger})] \\ &\quad + \alpha_{0,\rm p}[2-\kappa\chi_{\rm c,p}(0) - \kappa\chi_{\rm c,p}(\omega)]\tilde{\epsilon},\end{aligned} \tag{A21}$$

and the detected field quadrature can be written as

$$X_{\rm out} = -\frac{4}{\kappa}\alpha_{0,\rm p}\,C(\omega)[i\omega\tilde{\phi} + g_0(\tilde{b}+\tilde{b}^{\dagger})] + D(\omega)\tilde{\epsilon}, \tag{A22}$$

where

$$C(\omega) = i\frac{\kappa^2}{8}\left[\chi_{\rm c,p}(\omega)\chi_{\rm c,p}(0)e^{-i\theta_{\rm LO}} - \chi_{\rm c,p}^*(-\omega)\chi_{\rm c,p}^*(0)e^{i\theta_{\rm LO}}\right] \tag{A23}$$

and

$$\begin{aligned}D(\omega) = &\left(1-\frac{\kappa}{2}\chi_{\rm c,p}(\omega) - \frac{\kappa}{2}\chi_{\rm c,p}(0)\right)e^{-i\theta_{\rm LO}} \\ &+ \left(1-\frac{\kappa}{2}\chi_{\rm c,p}^*(-\omega) - \frac{\kappa}{2}\chi_{\rm c,p}^*(0)\right)e^{i\theta_{\rm LO}}.\end{aligned} \tag{A24}$$

In the particular case of phase quadrature detection with a resonant probe field (i.e., for $\Delta_{\rm p}=0$ and $\theta_{\rm LO}=\pi/2$) as, e.g., in the signal of a PDH detection, we find that $D(\omega)=0$ and $C(\omega)$ reduces to the usual cavity filtering function of Eq. (12). In the following, we consider this experimental situation, and in particular, since $D(\omega)=0$, we neglect the correlation between the mechanical fluctuations and the amplitude noise of the probe and the local oscillator.

It is useful to separate in $(\tilde{b}+\tilde{b}^{\dagger})$ the term proportional to $\tilde{\phi}$ from the expressions in the absence of phase noise. Using Eq. (A14) as well, we thus write

$$\begin{aligned}X_{\rm out} = -\frac{4}{\kappa}\alpha_{0,\rm p}\,C(\omega)\big[\{&i\omega + g_0^2\alpha_0^2\kappa\,[\chi_{\rm c}^*(0)\chi_{\rm c}(\omega) \\ &- \chi_{\rm c}(0)\chi_{\rm c}^*(-\omega)][-\chi_{\rm eff}(\omega) + \chi_{\rm eff}^*(-\omega)]\}\tilde{\phi} \\ &+ g_0(\tilde{b}+\tilde{b}^{\dagger})_{{\rm no}\,\phi}\big].\end{aligned} \tag{A25}$$

The symmetrized spectrum of $X_{\rm out}$, defined as $S_{\rm out} = \frac{1}{2}\int\frac{{\rm d}\omega'}{2\pi}\langle X_{\rm out}^{\dagger}(\omega')X_{\rm out}(\omega) + X_{\rm out}^{\dagger}(\omega')X_{\rm out}(-\omega)\rangle$, can be calculated from Eq. (A25). A simple and clear form is obtained in the weak-coupling limit (implying $\Gamma_{\rm eff} \ll \kappa, \Omega_{\rm m}$) by replacing $\omega \to \Omega_{\rm m}$ inside the square brackets, everywhere except in $\chi_{\rm eff}$, and neglecting the terms proportional to $\chi_{\rm eff}(\omega)\chi_{\rm eff}(-\omega)$. After some algebra, the output spectrum turns out to be proportional to the expression given in Eq. (11). The proportionality constant is removed using an additional calibration tone, i.e., a coherent phase modulation at a frequency far from $\Omega_{\rm m}$, yielding an additional peak in $S_{\nu\nu}$ which is used to determine the overall scale constant in the experimental spectrum.

[1] M. Aspelmeyer, T. J. Kippenberg, and F. Marquardt, Cavity optomechanics, Rev. Mod. Phys. **86**, 1391 (2014).

[2] W. Bowen and G. Milburn, *Quantum Optomechanics* (CRC Press, Boca Raton, FL, 2015).

[3] J. Chan, T. P. M. Alegre, A. H. Safavi-Naeini, J. T. Hill, A. Krause, S. Gröblacher, M. Aspelmeyer, and O. Painter, Laser cooling of a nanomechanical oscillator into its quantum ground state, Nature (London) **478**, 89 (2011).

[4] J. D. Teufel, T. Donner, D. Li, J. W. Harlow, M. S. Allman, K. Cicak, A. J. Sirois, J. D. Whittaker, K. W. Lehnert, and R. W. Simmonds, Sideband cooling of micromechanical motion to the quantum ground state, Nature (London) **475**, 359 (2011).

[5] A. H. Safavi-Naeini, J. Chan, J. T. Hill, T. P. M. Alegre, A. Krause, and O. Painter, Observation of quantum motion of a nanomechanical resonator, Phys. Rev. Lett. **108**, 033602 (2012).

[6] U. Delić, M. Reisenbauer, K. Dare, D. Grass, V. Vuletić, N. Kiesel, and M. Aspelmeyer, Cooling of a levitated nanoparticle to the motional quantum ground state, Science **367**, 892 (2020).

[7] A. Ranfagni, K. Børkje, F. Marino, and F. Marin, Two-dimensional quantum motion of a levitated nanosphere, Phys. Rev. Res. **4**, 033051 (2022).

[8] J. Piotrowski, D. Windey, J. Vijayan, C. Gonzalez-Ballestero, A. de los Ríos Sommer, N. Meyer, R. Quidant, O. Romero-Isart, R. Reimann, and L. Novotny, Simultaneous ground-state cooling of two mechanical modes of a levitated nanoparticle, Nat. Phys. **19**, 1009 (2023).

[9] L. Magrini, P. Rosenzweig, C. Bach, A. Deutschmann-Olek, S. G. Hofer, S. Hong, N. Kiesel, A. Kugi, and M. Aspelmeyer, Real-time optimal quantum control of mechanical motion at room temperature, Nature (London) **595**, 373 (2021).

[10] F. Tebbenjohanns, M. L. Mattana, M. Rossi, M. Frimmer, and L. Novotny, Quantum control of a nanoparticle optically levitated in cryogenic free space, Nature (London) **595**, 378 (2021).

[11] M. Kamba, R. Shimizu, and K. Aikawa, Optical cold damping of neutral nanoparticles near the ground state in an optical lattice, Opt. Express **30**, 26716 (2022).

[12] C. Whittle *et al.*, Approaching the motional ground state of a 10-kg object, Science **372**, 1333 (2021).

[13] J. Guo, R. Norte, and S. Gröblacher, Feedback cooling of a room temperature mechanical oscillator close to its motional ground state, Phys. Rev. Lett. **123**, 223602 (2019).

[14] J. Guo, J. Chang, X. Yao, and S. Gröblacher, Active-feedback quantum control of an integrated low-frequency mechanical resonator, Nat. Commun. **14**, 4721 (2023).

[15] S. A. Saarinen, N. Kralj, E. C. Langman, Y. Tsaturyan, and A. Schliesser, Laser cooling a membrane-in-the-middle system close to the quantum ground state from room temperature, Optica **10**, 364 (2023).

[16] G. Huang, A. Beccari, N. J. Engelsen, and T. J. Kippenberg, Room-temperature quantum optomechanics using an ultra-low noise cavity, arXiv:2309.15051.

[17] J. D. Thompson, B. M. Zwickl, A. M. Jayich, F. Marquardt, S. M. Girvin, and J. G. E. Harris, Strong dispersive coupling of a high-finesse cavity to a micromechanical membrane, Nature (London) **452**, 72 (2008).

[18] M. Underwood, D. Mason, D. Lee, H. Xu, L. Jiang, A. B. Shkarin, K. Børkje, S. M. Girvin, and J. G. E. Harris, Measurement of the motional sidebands of a nanogram-scale oscillator in the quantum regime, Phys. Rev. A **92**, 061801(R) (2015).

[19] R. W. Peterson, T. P. Purdy, N. S. Kampel, R. W. Andrews, P.-L. Yu, K. W. Lehnert, and C. A. Regal, Laser cooling of a micromechanical membrane to the quantum backaction limit, Phys. Rev. Lett. **116**, 063601 (2016).

[20] M. Rossi, D. Mason, J. Chen, Y. Tsaturyan, and A. Schliesser, Measurement-based quantum control of mechanical motion, Nature (London) **563**, 53 (2018).

[21] A. Borrielli, M. Bonaldi, E. Serra, A. Bagolini, P. Bellutti, F. S. Cataliotti, F. Marin, F. Marino, A. Pontin, G. A. Prodi, G. Pandraud, P. M. Sarro, G. Lorito, and T. Zoumpoulidis, Design of silicon micro-resonators with low mechanical and optical losses for quantum optics experiments, Microsyst. Technol. **20**, 907 (2014).

[22] A. Borrielli, L. Marconi, F. Marin, F. Marino, B. Morana, G. Pandraud, A. Pontin, G. A. Prodi, P. M. Sarro, E. Serra, and M. Bonaldi, Control of recoil losses in nanomechanical sin membrane resonators, Phys. Rev. B **94**, 121403(R) (2016).

[23] E. Serra, M. Bawaj, A. Borrielli, G. Di Giuseppe, S. Forte, N. Kralj, N. Malossi, L. Marconi, F. Marin, F. Marino, B. Morana, R. Natali, G. Pandraud, A. Pontin, G. A. Prodi, M. Rossi, P. M. Sarro, D. Vitali, and M. Bonaldi, Microfabrication of large-area circular high-stress silicon nitride membranes for optomechanical applications, AIP Adv. **6**, 065004 (2016).

[24] E. Serra, B. Morana, A. Borrielli, F. Marin, G. Pandraud, A. Pontin, G. A. Prodi, P. M. Sarro, and M. Bonaldi, Silicon nitride moms oscillator for room temperature quantum optomechanics, J. Microelectromech. Syst. **27**, 1193 (2018).

[25] E. Serra, A. Borrielli, F. Marin, F. Marino, N. Malossi, B. Morana, P. Piergentili, G. A. Prodi, P. M. Sarro, P. Vezio, D. Vitali, and M. Bonaldi, Silicon-nitride nanosensors toward room temperature quantum optomechanics, J. Appl. Phys. **130**, 064503 (2021).

[26] W. H. P. Nielsen, Y. Tsaturyan, C. B. Møller, E. S. Polzik, and A. Schliesser, Multimode optomechanical system in the quantum regime, Proc. Natl. Acad. Sci. USA **114**, 62 (2017).

[27] V. Dumont, S. Bernard, C. Reinhardt, A. Kato, M. Ruf, and J. C. Sankey, Flexure-tuned membrane-at-the-edge optomechanical system, Opt. Express **27**, 25731 (2019).

[28] P. Rabl, C. Genes, K. Hammerer, and M. Aspelmeyer, Phase-noise induced limitations on cooling and coherent evolution in optomechanical systems, Phys. Rev. A **80**, 063819 (2009).

[29] A. M. Jayich, J. C. Sankey, K. Børkje, D. Lee, C. Yang, M. Underwood, L. Childress, A. Petrenko, S. M. Girvin, and J. G. E. Harris, Cryogenic optomechanics with a Si_3N_4 membrane and classical laser noise, New J. Phys. **14**, 115018 (2012).

[30] A. H. Safavi-Naeini, J. Chan, J. T. Hill, S. Gröblacher, H. Miao, Y. Chen, M. Aspelmeyer, and O. Painter, Laser noise in cavity-optomechanical cooling and thermometry, New J. Phys. **15**, 035007 (2013).

[31] V. Sudhir, D. J. Wilson, R. Schilling, H. Schütz, S. A. Fedorov, A. H. Ghadimi, A. Nunnenkamp, and T. J. Kippenberg, Appearance and disappearance of quantum correlations in measurement-based feedback control of a mechanical oscillator, Phys. Rev. X **7**, 011001 (2017).

[32] P. Vezio, An experimental setup for quantum optomechanics, Ph.D. thesis, University of Florence, 2021; https://flore.unifi.it/handle/2158/1234350.

[33] A. Pontin, M. Bonaldi, A. Borrielli, L. Marconi, F. Marino, G. Pandraud, G. A. Prodi, P. M. Sarro, E. Serra, and F. Marin,

Quantum nondemolition measurement of optical field fluctuations by optomechanical interaction, Phys. Rev. A **97**, 033833 (2018).

[34] R. A. Norte, J. P. Moura, and S. Gröblacher, Mechanical resonators for quantum optomechanics experiments at room temperature, Phys. Rev. Lett. **116**, 147202 (2016).

[35] Y. Tsaturyan, A. Barg, E. S. Polzik, and A. Schliesser, Ultracoherent nanomechanical resonators via soft clamping and dissipation dilution, Nat. Nanotechnol. **12**, 776 (2017).

[36] O. Arcizet, C. Molinelli, T. Briant, P.-F. Cohadon, A. Heidmann, J.-M. Mackowski, C. Michel, L. Pinard, O. Français, and L. Rousseau, Experimental optomechanics with silicon micromirrors, New J. Phys. **10**, 125021 (2008).

[37] Y. Levin, Internal thermal noise in the LIGO test masses: A direct approach, Phys. Rev. D **57**, 659 (1998).

[38] V. Braginsky, M. Gorodetsky, and S. Vyatchanin, Thermodynamical fluctuations and photo-thermal shot noise in gravitational wave antennae, Phys. Lett. A **264**, 1 (1999).

[39] V. Braginsky, M. Gorodetsky, and S. Vyatchanin, Thermo-refractive noise in gravitational wave antennae, Phys. Lett. A **271**, 303 (2000).

[40] M. L. Gorodetsky, Thermal noises and noise compensation in high-reflection multilayer coating, Phys. Lett. A **372**, 6813 (2008).

[41] S. A. Fedorov, A. Beccari, A. Arabmoheghi, D. J. Wilson, N. J. Engelsen, and T. J. Kippenberg, Thermal intermodulation noise in cavity-based measurements, Optica **7**, 1609 (2020).

[42] C. M. Pluchar, A. R. Agrawal, and D. J. Wilson, Thermal intermodulation backaction in a high-cooperativity optomechanical system, Optica **10**, 1543 (2023).